

# Opening of the human epithelial calcium channel TRPV6

Luke L. McGoldrick<sup>1,2\*</sup>, Appu K. Singh<sup>1\*</sup>, Kei Saotome<sup>1</sup>, Maria V. Yelshanskaya<sup>1</sup>, Edward C. Twomey<sup>1,2</sup>, Robert A. Grassucci<sup>1</sup> & Alexander I. Sobolevsky<sup>1</sup>

Calcium-selective transient receptor potential vanilloid subfamily member 6 (TRPV6) channels play a critical role in calcium uptake in epithelial tissues<sup>1–4</sup>. Altered TRPV6 expression is associated with a variety of human diseases<sup>5</sup>, including cancers<sup>6</sup>. TRPV6 channels are constitutively active<sup>1,7,8</sup> and their open probability depends on the lipidic composition of the membrane in which they reside; it increases substantially in the presence of phosphatidylinositol 4,5-bisphosphate<sup>7,9</sup>. Crystal structures of detergent-solubilized rat TRPV6 in the closed state have previously been solved<sup>10,11</sup>. Corroborating electrophysiological results<sup>3</sup>, these structures demonstrated that the  $\text{Ca}^{2+}$  selectivity of TRPV6 arises from a ring of aspartate side chains in the selectivity filter that binds  $\text{Ca}^{2+}$  tightly. However, how TRPV6 channels open and close their pores for ion permeation has remained unclear. Here we present cryo-electron microscopy structures of human TRPV6 in the open and closed states. The channel selectivity filter adopts similar conformations in both states, consistent with its explicit role in ion permeation. The iris-like channel opening is accompanied by an  $\alpha$ -to- $\pi$ -helical transition in the pore-lining transmembrane helix S6 at an alanine hinge just below the selectivity filter. As a result of this transition, the S6 helices bend and rotate, exposing different residues to the ion channel pore in the open and closed states. This gating mechanism, which defines the constitutive activity of TRPV6, is, to our knowledge, unique among tetrameric ion channels and provides structural insights for understanding their diverse roles in physiology and disease.

We expressed the full-length human TRPV6 (hTRPV6) channel in HEK 293 cells, where it exhibited typical  $\text{Ca}^{2+}$  permeability<sup>12</sup> (Fig. 1a, b) and current–voltage relationships<sup>13–17</sup> (Extended Data Fig. 1a). To structurally characterize hTRPV6, we purified it separately in nanodiscs and amphipols (see Methods) and solved the corresponding structures using cryo-electron microscopy (cryo-EM; Extended Data Figs 2, 3 and Extended Data Table 1) to 3.6 Å and 4.0 Å, respectively. Although the reconstructions in nanodiscs and amphipols were nearly identical, the structure solved in nanodiscs had better overall resolution and will be our primary descriptor of hTRPV6. Two-dimensional class averages showed diverse orientations and easily discernible secondary structure features (Fig. 1c). The resulting 3D reconstruction (Fig. 1d, e) showed higher resolution features for the core of the molecule than for its periphery (Extended Data Fig. 2c) and was of sufficient quality (Extended Data Fig. 4) to build each subunit (residues 28–638) of the hTRPV6 homotetramer *de novo*.

The structure of hTRPV6 (Fig. 2a, b) has the same overall architecture as that of rat TRPV6 (rTRPV6)<sup>10</sup>. Whereas no discernible lipid densities were observed in the crystal structures of rTRPV6<sup>10,11</sup>, the hTRPV6 cryo-EM reconstruction reveals 16 (4 per subunit) well-resolved non-protein densities that are intercalated in subunit interfaces and are likely to represent lipids (Fig. 2c). Similarly positioned densities

in the structure of TRPV1<sup>18</sup> were modelled with phosphatidylinositol, phosphatidylcholine and phosphatidylethanolamine lipids. Of the four putative lipid densities in hTRPV6, the fourth density has a clear

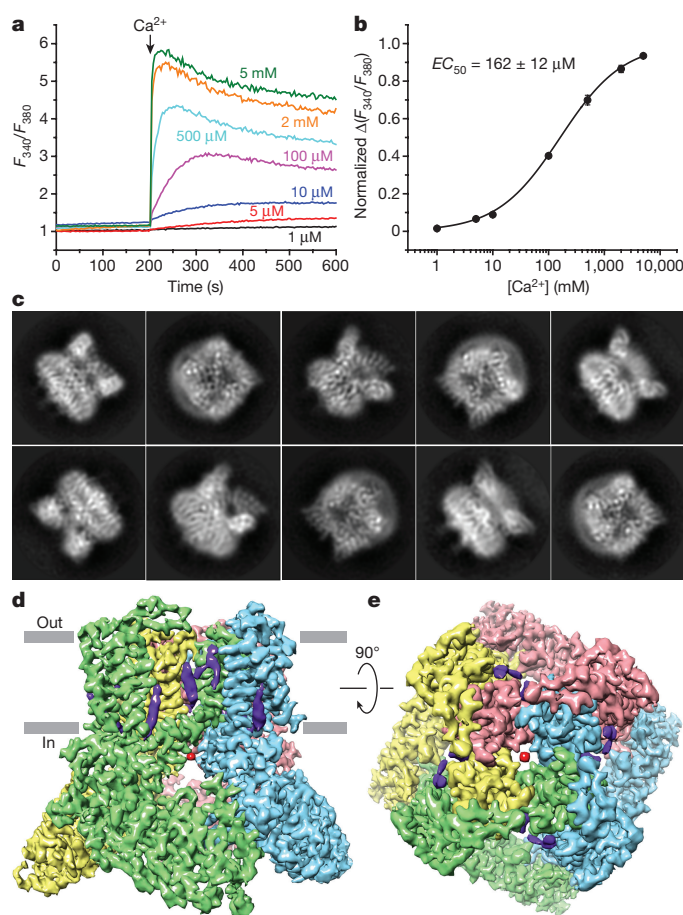


**Figure 1 | Function and cryo-EM of hTRPV6.** **a, b**, Functional characterization of hTRPV6 using ratiometric fluorescence measurements. **a**, Fluorescence curves recorded from HEK 293 cells expressing hTRPV6 in response to the application of  $\text{Ca}^{2+}$  (arrow) at different concentrations. These experiments were repeated independently three times with similar results. **b**,  $\text{Ca}^{2+}$  dose–response curve for the maximal value of fluorescence fitted with the logistic equation. The calculated half maximal effective concentration ( $\text{EC}_{50}$ ) is shown as mean  $\pm$  s.e.m. ( $n=3$ ). **c**, Two-dimensional class averages of hTRPV6 particles, showing diverse orientations. **d, e**, hTRPV6 3.6 Å cryo-EM reconstruction, with density shown at 0.035 threshold level (UCSF Chimera) representing hTRPV6 subunits coloured green, cyan, pink and yellow, lipid in purple and ions in red.

<sup>1</sup>Department of Biochemistry and Molecular Biophysics, Columbia University, 650 West 168th Street, New York, New York 10032, USA. <sup>2</sup>Integrated Program in Cellular, Molecular, and Biomedical Studies, Columbia University, 650 West 168th Street, New York, New York 10032, USA.

\*These authors contributed equally to this work.